

PAPER

Surface nanostructures on Nb-doped SrTiO₃ irradiated with swift heavy ions at grazing incidence

To cite this article: N Ishikawa *et al* 2022 *Nanotechnology* **33** 235303

View the [article online](#) for updates and enhancements.

You may also like

- [On the threshold for ion track formation in CaF₂](#)
M Karlušić, C Ghica, R F Negrea *et al.*
- [Response of GaN to energetic ion irradiation: conditions for ion track formation](#)
M Karlušić, R Kozubek, H Lebius *et al.*
- [Experimental evidence of crystalline hillocks created by irradiation of CeO₂ with swift heavy ions: TEM study](#)
N Ishikawa, N Okubo and T Taguchi



The Electrochemical Society
Advancing solid state & electrochemical science & technology

242nd ECS Meeting

Oct 9 – 13, 2022 • Atlanta, GA, US

Abstract submission deadline: **April 8, 2022**

Connect. Engage. Champion. Empower. Accelerate.

MOVE SCIENCE FORWARD



Submit your abstract



Surface nanostructures on Nb-doped SrTiO₃ irradiated with swift heavy ions at grazing incidence

N Ishikawa¹ , Y Fujimura¹, K Kondo¹, G L Szabo² , R A Wilhelm² ,
H Ogawa¹ and T Taguchi³

¹Nuclear Science and Engineering Center, Japan Atomic Energy Agency (JAEA), Tokai, Ibaraki 319-1195, Japan

²TU Wien, Institute of Applied Physics, A-1040 Vienna, Austria

³Quantum Beam Science Research Directorate, National Institutes for Quantum Science and Technology (QST), Tokai, Ibaraki 319-1106, Japan

E-mail: ishikawa.norito@jaea.go.jp

Received 4 January 2022, revised 17 February 2022

Accepted for publication 25 February 2022

Published 17 March 2022



CrossMark

Abstract

A single crystal of SrTiO₃ doped with 0.5 wt% niobium (Nb-STO) was irradiated with 200 MeV Au³²⁺ ions at grazing incidence to characterize the irradiation-induced hillock chains. Exactly the same hillock chains are observed by using atomic force microscopy (AFM) and scanning electron microscopy (SEM) to study the relation between irradiation-induced change of surface topography and corresponding material property changes. As expected, multiple hillocks as high as 5–6 nm are imaged by AFM observation in tapping mode. It is also found that the regions in between the adjacent hillocks are not depressed, and in many cases they are slightly elevated. Line-like contrasts along the ion paths are found in both AFM phase images and SEM images, indicating the formation of continuous ion tracks in addition to multiple hillocks. Validity of preexisting models for explaining the hillock chain formation is discussed based on the present results. In order to obtain new insights related to the ion track formation, cross-sectional transmission electron microscopy (TEM) observation was performed. The ion tracks in the near-surface region are found to be relatively large, whereas buried ion tracks in the deeper region are relatively small. The results suggest that recrystallization plays an important role in the formation of small ion tracks in the deep region, whereas formation of large ion tracks in the near-surface region is likely due to the absence of recrystallization. TEM images also show shape deformation of ion tracks in the near-surface region, suggesting that material transport towards the surface is the reason for the absence of recrystallization.

Keywords: swift heavy ion, hillocks, ion-tracks, ion irradiation, TEM, AFM, SEM

(Some figures may appear in colour only in the online journal)

1. Introduction

Continuous nanometer-sized damages, called ion tracks, can be created in ceramics, when they are irradiated with swift heavy ions (SHIs). Since sufficiently high electronic stopping power (S_e) is the prerequisite for ion track formation, the formation is likely to be triggered by energy deposition from SHIs into the electronic system of the materials [1–3]. The mechanism of ion track formation has been extensively

studied so far, since it has been one of the central topics in the research of ion-solid interactions over recent years. The ion track formation is often accompanied by the nanometer-sized surface protrusions called hillocks [4–12]. In case ceramics are irradiated with SHIs at normal incidence, a single hillock is formed at the incident surface by each ion impact. In contrast, when ceramics are irradiated with SHIs at grazing incidence, multiple hillocks in a chain can be created along the ion trajectory [13–22]. Formation of hillock chains was

first reported on SrTiO₃ (STO) [13], and later it has been reported also on several other ceramics, such as TiO₂ [18, 19], SiO₂ [20, 21] and STO doped with niobium [22]. Since the intermittent feature of hillock chains created at the surface is in contrast to continuous feature of ion tracks created in the bulk, it is not straightforward to relate the mechanism of hillock chain formation to that of ion track formation in the bulk. Therefore, the origin of the unique feature of hillock chains is still under debate.

In the present study, STO doped with 0.5wt% niobium (Nb-STO) is adopted to study the mechanism of hillock chains. Among the materials that are known to create hillock chains, Nb-STO is an interesting material having the same crystal structure with STO, while it has much higher electrical conductivity than STO. For example, STO doped with 0.5wt% niobium has an electrical conductivity higher than non-doped STO by 9 orders of magnitude [23]. High electrical conductivity of Nb-STO enables us to observe the surface morphology by scanning electron microscopy (SEM) without additional surface treatment. Since surface coating with conductive substances may alter the surface morphology, we believe conducting Nb-STO rather than insulating STO should be used for SEM studies. It should be pointed out here that the Nb-doping up to 1wt% has no evident influence on track formation according to the previous study of transmission electron microscopy (TEM) and small-angle x-ray scattering (SAXS) [24]. Moreover, our recent TEM study has shown that the sizes of ion tracks and hillocks in Nb-STO are similar to those in STO [25]. Therefore, Nb-STO can be a good surrogate of STO for studying the mechanism of hillock chain formation.

In the present study, Nb-STO is irradiated with 200 MeV Au ions at grazing angle (0.5–1.0 degree). Atomic force microscopy (AFM) observation of hillock chains is performed in tapping mode. The height information allows us to observe the irradiation-induced surface topography, whereas the phase information is used to map corresponding material property changes. Measurements using SEM are also performed to obtain complementary information of a surface topography and material property changes related to hillock chain formation. The unique strategy of the present study is that exactly the same hillock chains are observed using these techniques. To obtain additional insight related to ion tracks created by the irradiation at grazing incidence, cross-sectional TEM observation was also performed.

2. Experiments

A single crystal of 0.5 wt% niobium-doped SrTiO₃ (100) (Nb-STO) (commercially acquired from Shinkosha Co., Ltd, Japan) were irradiated with 200 MeV Au³²⁺ ions at grazing incidence at room temperature in the tandem accelerator at JAEA-Tokai (Japan Atomic Energy Agency, Tokai Research and Development Center). To achieve grazing incidence of the ion beam, a sample was mounted on a sample holder which is aligned almost parallel to the beamline. As a result, grazing angle close to zero was achieved. The angle between

beam direction and the sample surface was estimated to be in the range of 0.5–1.0 degree. The estimation procedure of the irradiation angle will be explained later. The charge state (32+) was chosen so that the charge of the incident ions is the same as the average value of the equilibrium charge. To avoid overlapping of individual hillock chains, the fluence was chosen to yield 2–3 impacts per μm^2 .

To observe exactly the same hillock chains using AFM and SEM, they were at first observed by AFM in the designated area prior to SEM observation. For example, the area two millimeter distant from the edge of the sample was observed by AFM. Several AFM images were taken with different magnifications, so that we can identify in which area the specific hillock chains are located. After the AFM observation, we searched the hillock chains by SEM using the AFM results, and SEM observation were performed for the hillock chains that are observed by AFM.

The as-irradiated sample was observed with AFM (Asylum research cypher scanning probe microscope) in tapping mode with a spring constant in the range of 1.0–3.5 N m⁻¹. The phase images yield information on variations in surface properties such as adhesive, stiffness or frictional properties. Although it is difficult to specify which property change is attributed to the phase shift, the phase imaging technique is a sensitive method to map material modification caused by the irradiation [26]. To examine the reliability of the AFM observation, the probe tip (Olympus Micro Cantilever, Type: OMCL AC240TS R3) used in the present AFM study was observed by SEM (SIGMA, Carl Zeiss Microscopy, Germany). The energy of the electron beam was 5 keV for the SEM observation of the probe tip.

The as-irradiated surface was also observed by SEM. By observing exactly the same hillocks using AFM and SEM, irradiation-induced topological change and corresponding property change were directly compared. The energy of the electron beam was 3 keV for the observations of the sample.

To prepare a TEM sample, the as-irradiated sample was coated with a protective osmium layer, and then a cross-sectional TEM lamella sample was prepared by the focused ion beam (FIB) lift-out technique using a 40 keV Ga ion beam from the NB5000 (Hitachi High-Tech Corporation). The lamella sample was cut perpendicular to the irradiation direction, so that cross-section of ion tracks can be observed. TEM images were taken with the following two equipments. The low magnification TEM images were taken with a HF3300 (Hitachi High-Tech Corporation) operated at 300 kV, and the magnified TEM images were taken with a 2100F (JEOL Ltd) operated at 200 kV. According to the SRIM-2010 code [27, 28], the electronic stopping power (S_e) of the 200 MeV Au beam in Nb-STO was estimated to be 28.6 keV nm⁻¹.

3. Results and discussion

3.1. Results of AFM and SEM observations

A height image of the AFM observation (figure 1(a)) shows dotted contrasts aligned in the direction of irradiation,

indicating the formation of hillock chains. Figure 1(b) shows a height profile analyzed along the irradiation direction. It demonstrates that many of the multiple hillocks are as high as 5–6 nm, and they are separated by the interval of around 30–50 nm. The length of the hillock chains is in the range of about 0.5–1.0 μm . It corresponds to the incidence angle in the range of about 0.5–1.0 degree relative to surface according to the length-angle relationship reported in [13]. Figure 1(c) shows the height profile analyzed perpendicular to the irradiation direction. It shows the height profile in between the adjacent hillocks. The regions in between the hillocks are not depressed, and the regions in between the hillocks are found to be slightly elevated. Although in the previous literature the region was assumed to be depressed based on the SEM observation [22], the present AFM observation clearly shows that the regions are not depressed.

In order to confirm the absence of depressed region, line profile analyses were performed for some of the hillock chains as shown in figure 2. The figures again demonstrate that a depressed region in between the adjacent hillocks is not observed, and the elevated regions in between the adjacent hillocks are often observed. Sometimes the elevation cannot be resolved in the AFM image, since they are in the range of the surface roughness. Nevertheless, it can be concluded that the regions in between the adjacent hillocks are not depressed for all cases.

It should be noted that AFM measurements may involve systematic errors of a few nanometers due to the finite size of probe tips [9,29–32]. If the tip diameter is comparable to the distance between adjacent hillocks, the observation of the elevated region in between hillocks becomes questionable. To confirm the probe tip is sufficiently sharp, the probe tip used in the present AFM observation was observed by SEM. As shown in figure 3, the SEM image of the probe tip shows the tip diameter is around 10 nm. Since the tip diameter is smaller than the distance between consecutive hillocks by a factor of 3–5, we can conclude that the regions in between the hillocks are never depressed.

As shown in figure 4, the phase image of AFM observation shows dot-like contrasts of multiple hillocks similar to those observed in the height image. The image also shows line-like contrasts parallel to the irradiation direction. As far as we have observed, dot-like contrasts are always accompanied with line-like contrasts. The line-like contrasts indicate continuous modification of materials property along the ion path, suggesting that ion tracks are created continuously in the near-surface region.

Similar to the AFM phase image, the SEM image (figure 5) also exhibits both line-like features of ion tracks and dot-like features of hillock chains. It is interesting to see that the hillocks are observed as circles rather than elongated dots. The direct comparison of AFM images and a SEM image is shown in figure 6. The length of the line-like contrasts observed in the SEM image is similar to that observed in the AFM phase image. It should be reminded here that ion track should be created not only in near-surface region but also in deeper region. This means that it is likely that both SEM and AFM can detect nearly the same modified region (i.e. only a

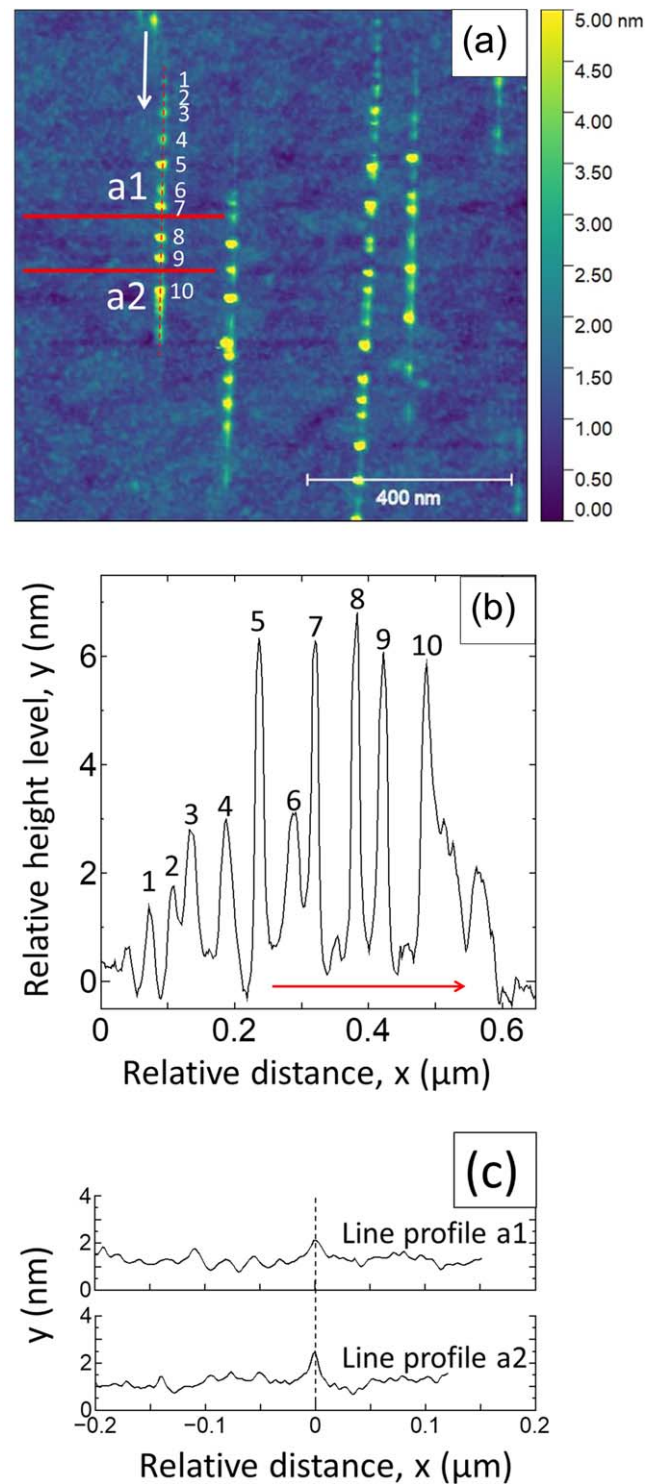


Figure 1. (a) AFM height image for Nb-STO irradiated with 200 MeV Au ions at grazing incidence. The arrow indicates the irradiation direction. The dashed vertical line indicates the line where the line profile parallel to irradiation direction is analyzed. The solid horizontal lines indicate the lines where the line profile perpendicular to irradiation direction is analyzed. Numbers (1–10) are assigned for each hillock to facilitate the comparison between figures 1(a) and (b). (b) Height profile analyzed along the red dotted line shown in figure 1(a). The arrow indicates the irradiation direction. The numbers (1–10) indicated in the figure correspond to those indicated in figure 1(a). (c) Height profiles analyzed along the solid lines shown in figure 1(a). The relative distance (x) is the distance from the ion trajectory, where the location of the ion trajectory corresponds to $x = 0$.

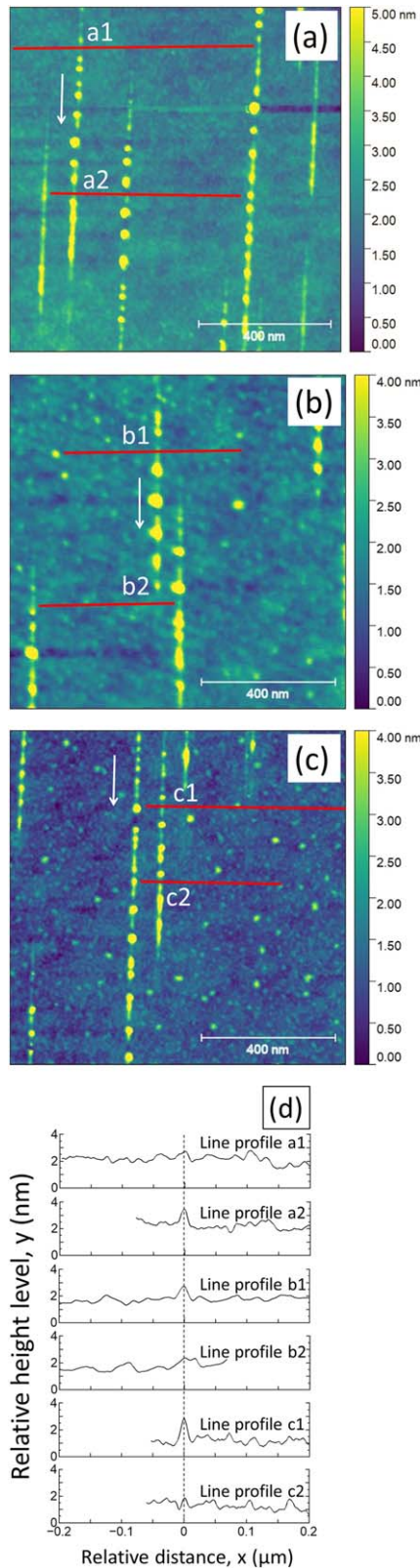


Figure 2. (a)–(c) AFM height images for Nb-STO irradiated with 200 MeV Au ions at grazing incidence. The arrows in figures 2(a)–(c) indicate the irradiation direction. The solid horizontal lines indicate the lines where the line profile perpendicular to irradiation direction is analyzed. (d) Height profiles analyzed along the solid lines shown in figures 2(a)–(c). The relative distance (x) is the distance from the ion trajectory, where the location of the ion trajectory corresponds to $x = 0$.

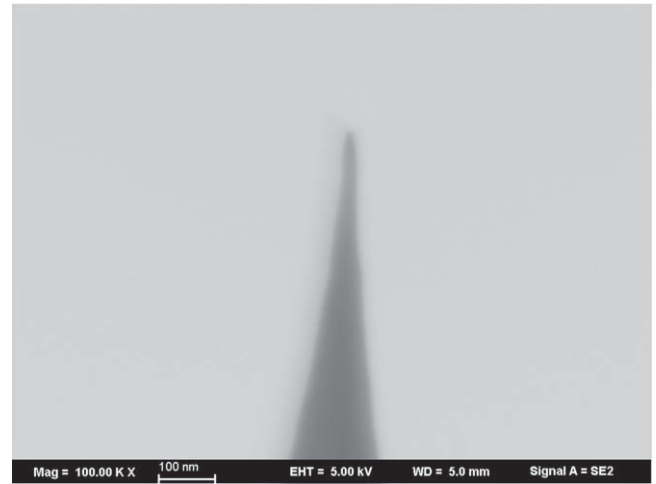


Figure 3. SEM image of the probe tip used for the present AFM observations.

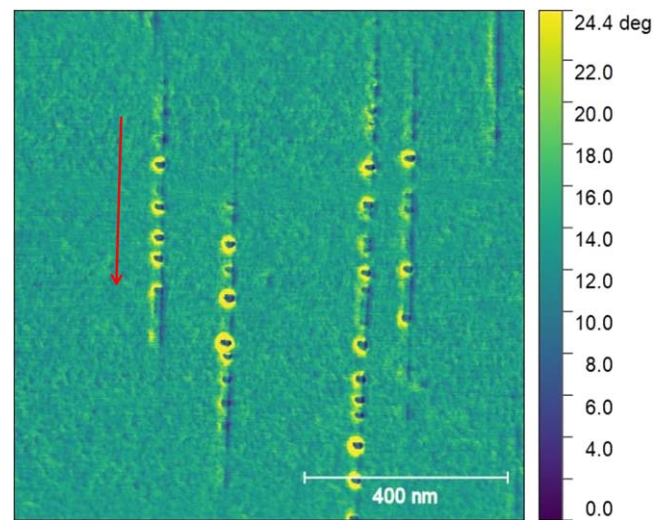


Figure 4. AFM phase image for Nb-STO irradiated with 200 MeV Au ions at grazing incidence. The arrow indicates the irradiation direction. The same area as that shown in figure 1(a) were observed.

near-surface part of the ion tracks). Conversely, they cannot detect irradiation-induced modification in deeper region. Since SEM is sensitive to not only topographic feature of the surface but also sample properties affecting the secondary electron yield, the interpretation of SEM images is not straightforward. It is important to note that there is a tendency that dot-like contrasts in the SEM image are clearly visible, when hillocks are high. Although small hillocks having low height are recognizable in the AFM images, some of them are not recognizable in the SEM image. These results suggest that SEM is less sensitive to topographic feature of the surface than AFM.

3.2. Results of TEM observation

The low magnification TEM image (figure 7) shows that ion tracks are created not only in the near-surface region but also in deeper regions. The tracks in the near-surface region are

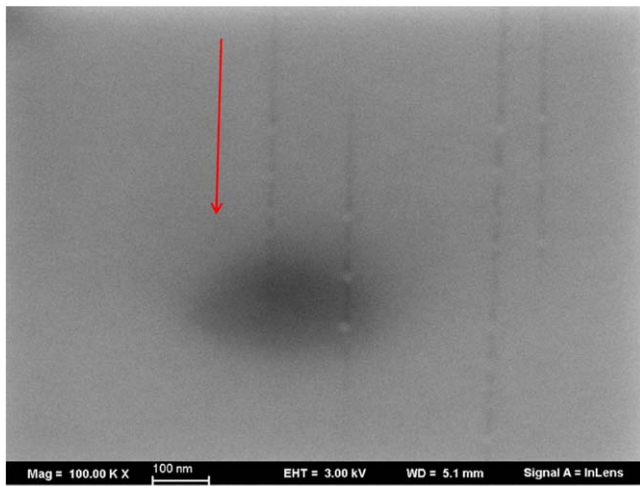


Figure 5. SEM image of Nb-STO irradiated with 200 MeV Au ions at grazing incidence. The arrow indicates the irradiation direction. The same area as that shown in figure 1(a) were observed.

relatively large. The tracks in the deep region are relatively small, and they are recognizable at least to the depth of around 100 nm. In figure 8, several track images are displayed in the order of the depth of the ion track. Large tracks with a diameter of about 10 nm are located at the near-surface region up to the depth of about 15 nm, whereas small tracks with diameters of about 5 nm or less are found at the deeper regions, i.e. at a depth of 25 nm and more. The results suggest the existence of a critical depth where the track size abruptly changes.

It is also found that the track shape evolves depending on the depth. Figures 8(a)–(d) show that the tracks are deformed towards the surface. The track deformation suggests that material transport toward surface takes place, when the ion tracks are created in the near-surface region. Figure 8(d) demonstrates that the track deformation occurs even at the depth of about 15 nm which is larger than the track diameter. It is likely that the track deformation is closely related to the formation of large ion tracks, whereas the absence of deformation is related to the formation of small ion tracks. The correlation will be discussed in the next section

3.3. Discussion

3.3.1. Mechanism of hillock chain formation. It is known that the mechanism of ion track formation is deeply related to the energy deposition of SHIs into the electronic system of the target material. According to our previous TEM study [25], continuous ion tracks are formed in STO and Nb-STO irradiated with SHIs at large-angle incidence. The continuous feature of the ion tracks reflects continuous energy deposition along the ion paths. On the other hand, the present study shows that the hillock chains exhibit intermittent features (i.e. formation of multiple hillocks) and at the same time continuous features (i.e. formation of a line-like modified region). Therefore, the preexisting models to account for the

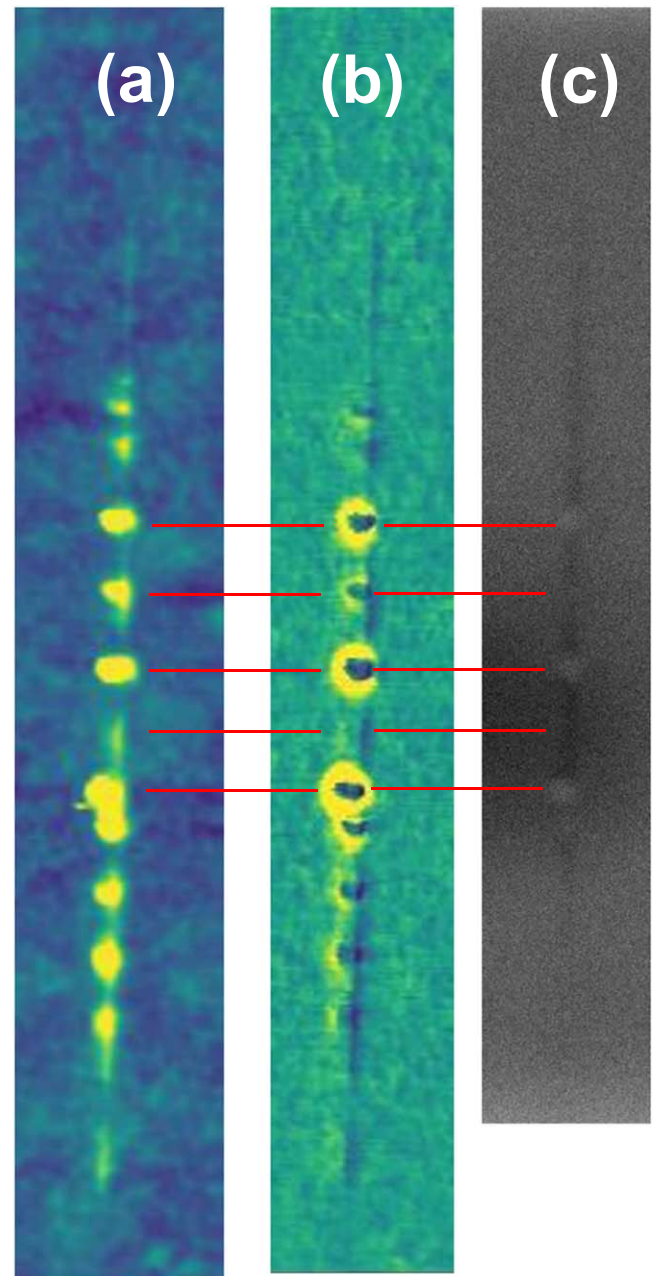


Figure 6. Comparison of (a) AFM height image, (b) AFM phase image and (c) SEM image in Nb-STO irradiated with 200 MeV Au ions at grazing incidence. The images are taken for the same hillock chain. Red lines are eyeguides to specify the location of hillocks.

continuous ion track formation have to be altered in order to account for the unique features of hillock chains.

So far, two models have been proposed to account for the hillock chain formation. One of the models assumes sharply peaked energy deposition which occurs periodically along the ion trajectory. Since the electron density is much higher on the TiO₂ layers than on the SrO layers, peaks of electronic energy deposition can take place repeatedly as the travelling ion passes the TiO₂ layers [13–16]. Multiple peaks of energy deposition can explain the periodic formation of multiple hillocks. The new insight obtained by the present results is that the energy deposition in between the position of energy

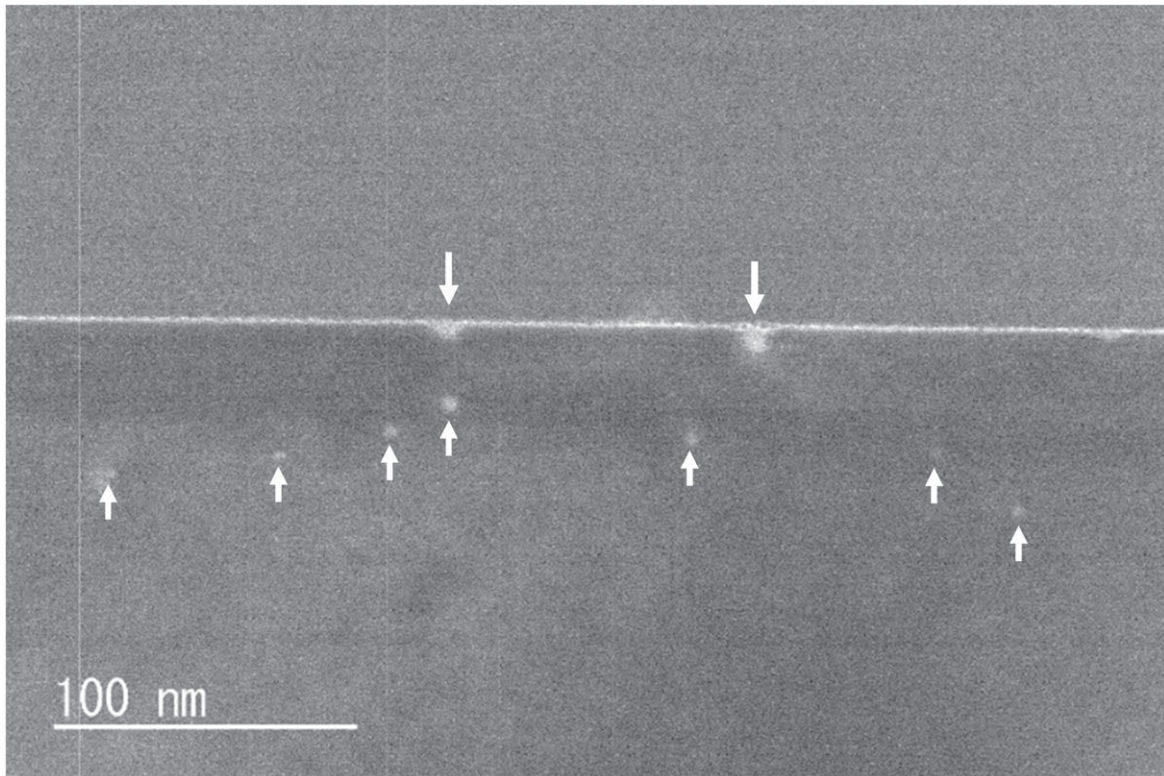


Figure 7. Low magnification image of the cross-sectional TEM measurement in Nb-STO irradiated with 200 MeV Au ions at grazing incidence. The arrows pointing down indicate ion tracks created in the near-surface region, whereas the arrows pointing up indicate ion tracks created in the deep region.

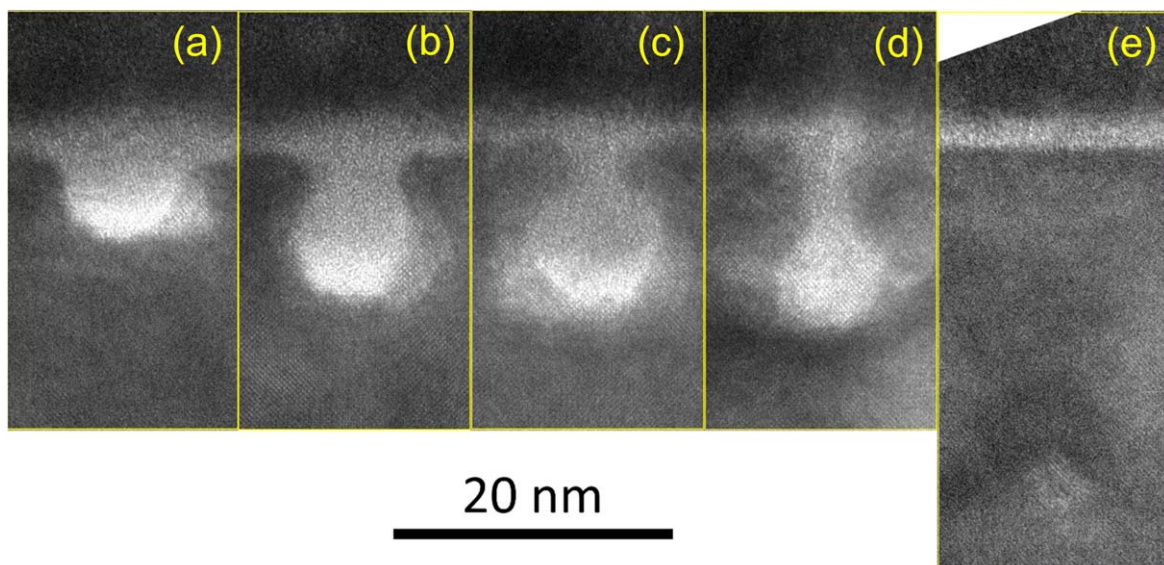


Figure 8. High magnification images of the cross-sectional TEM measurement in Nb-STO irradiated with 200 MeV Au ions at grazing incidence. The images are displayed in order of depth of the ion tracks to examine the depth-dependence of the ion track size and shape.

deposition peaks should be sufficiently high to cause line-like modification together with slight elevation of the surface. This means that a small amount of transiently molten region has to be continuously formed in between the adjacent hillocks. Although the magnitude of energy deposition is largely dependent on the trajectory of the ions, high S_e sufficient to cause slight elevation of surface with additional peaks of S_e to

form multiple hillocks can be explained in the framework of this model [16].

Another model to account for the hillock chain formation assumes a Rayleigh instability [22]. The model is based on the continuous energy deposition which can at least explain the formation of line-like contrasts at the irradiated surface. According to the Rayleigh instability theory [33], the molten

region along the ion path can break up into smaller packets, and the formation of multiple droplets can explain the formation of multiple hillocks. The previous SEM study [22] has suggested groove formation along the ion trajectories, and it was the basis of supporting the Rayleigh instability scenario. However, the present result of AFM observation demonstrates that the line-like contrasts correspond to either slightly elevated regions or regions having the same roughness as that of the matrix. They never exhibit depressed feature. Therefore, the validity of the Rayleigh instability model appears to be questionable.

3.3.2. Large and deformed ion tracks in the near-surface region. The present results mentioned above demonstrate the importance of elucidating the relationship between multiple hillocks and line-like modified regions namely ion tracks. However, the characterization of the ion tracks created by the irradiation at grazing incidence is still lacking.

At first, it is important to remind the characteristics of hillocks and ion tracks created by irradiation at large-angle incidence. According to the previous TEM results of Nb-STO irradiated at 45 degree incidence [25], hillocks are formed by the protrusion of the transiently molten region near ion path, leading to the formation of hillocks ($D_{\text{hillock}} = 11\text{--}13$ nm) as large as the molten region. On the other hand, relatively small ion tracks ($D_{\text{track}} = 3\text{--}4$ nm) are created in the bulk, and their formation can be explained by transient melting with successive partial recrystallization. The previous studies of ion track formation in non-amorphizable ceramics also show that transient melting and successive recrystallization is the likely origin of the formation of ion tracks that are smaller than the transiently molten region [34–39].

It is important to note that the size of small ion tracks in the deep region observed in the present study ($D_{\text{track}} \leq 5$ nm) is similar to that of ion tracks observed in Nb-STO irradiated with 200 MeV Au ions at a large-angle (45 degrees) of incidence ($D_{\text{track}} = 3\text{--}4$ nm) [25]. Therefore, the recrystallization scenario is applicable to interpret the present results. For example, the ion tracks in the deeper region with a diameter of $D \leq 5$ nm are relatively small, and it is indicative of transient melting and subsequent recrystallization. On the other hand, the large tracks with a diameter of $D \sim 10$ nm are observed in the near-surface region, and it seems that recrystallization is absent in this case.

According to the present TEM results, large ion tracks in the near-surface region are accompanied with a shape deformation of tracks, whereas small ion tracks in the deep region are not deformed. Therefore, the large ion track in the near-surface region is likely to be related to the deformation of the ion tracks. The ion tracks in the near-surface region are deformed towards the surface, suggesting that the material transport takes place towards the surface during transient melting. Such material transport can result in material deficiency, which hinders the molten region to recrystallize. Therefore, relatively large ion tracks can be explained as a consequence of transient melting and failure of recrystallization.

3.3.3. Possible factors affecting the track formation. Here, it is worth discussing the possible surface effects related to track formation. One of the possible surface effects is slower cooling rate near-surface than that in the bulk. Heat dissipation is limited near-surface, while heat of the molten region surrounded by cold matrix can be efficiently dissipated. The previous molecular simulation for CaF_2 irradiated with swift heavy ions has demonstrated that the bulk part of the track is cooled fast due to a heat sink into the surrounding matrix, while the protruded part remains liquid for a longer time period (~ 60 ps) [35]. Such slow cooling rate is favorable for damage recovery during cooling via recrystallization process. However, the present study shows the contradicting result showing that tracks in the near-surface region are larger than those in the deep region. The contradiction has to be reconciled. Here, it should be noted that slower cooling rate leads to longer lifetime of the melt, resulting in longer time period for material transport. Therefore, there seems to be two competing surface effects related to track formation, i.e. high recrystallization efficiency due to slow cooling rate versus significant material loss due to material transport toward surface. The former effect is favorable for damage recovery, while the latter effect hinders damage recovery.

It is important to remind that conical tracks are formed near-surface in TiO_2 irradiated with swift heavy ions at *normal* incidence [40]. According to the study, conical tracks as long as 60–70 nm are formed below the surface, while hillocks are formed at the end of the tracks. The study has concluded that the material is removed from the conical volume to form a surface hillock, suggesting that the material transport toward surface during melting is important for the formation of the conical track. In this case, the effect of material loss is dominant rather than that of slow cooling rate near-surface. On the other hand, the bulk part of tracks is recovered via recrystallization in TiO_2 , indicating that material loss is very small in the deep region. The results are in line with the present result of Nb-STO irradiated with swift heavy ions at grazing incidence, since the present result also suggests the importance of material transport for the formation of large tracks in the near-surface region.

Another possible surface effect contributing to track formation is the enhancement of energy deposition due to imperfection of crystal lattice. According to the previous study [41], the track size increases with the density of pre-existing defects in STO, suggesting that the energy deposition to the lattice system increases by the decrease in the electronic and atomic thermal conductivities and increase in electron-phonon coupling. Since the presence of surface may also contribute to the increase in energy deposition in the similar manner to that of pre-existing defects, such surface effects should be also taken into account.

On the other hand, the track formation in the region far from the surface (in the deep region) can be simply interpreted by the transient melting followed by partial recrystallization. The efficiency of recrystallization in the bulk can be dependent on various material factors, such as ionic bonding character [42, 43], the diffusion velocity of

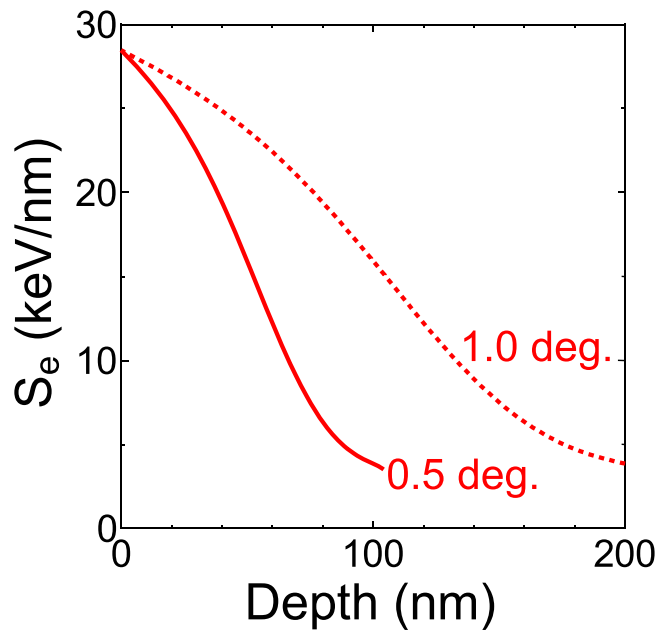


Figure 9. Depth dependence of S_e in Nb-STO irradiated with 200 MeV Au ions at grazing incidence. The solid curve shows depth dependence of S_e assuming the grazing angle of 0.5 degrees, whereas the dotted curve assumes the grazing angle of 1.0 degree.

anion atoms [37], simplicity of lattice structure [34] and viscosity [34]. Since the present study shows formation of relatively small ion tracks in the bulk, high recrystallization efficiency is suggested for Nb-STO. It should be mentioned here that the relationship between recrystallization efficiency and material factors mentioned above should be further studied in future for wide range of materials. The validity of the relationship should be examined within a limited experimental condition that material transport is negligibly small, since the material transport can significantly affect the track formation as demonstrated in the present study.

3.3.4. Relation between depth-dependence of S_e and that of track size. It is worth noting here that the depth-dependence of S_e should be taken into account when analyzing the depth-dependence of the track size. Based on the result of SRIM calculation, the depth-dependence of S_e is plotted in figure 9. According to [17], the track size in STO decreases with decreasing S_e , and the threshold S_e of track formation is around 10 keV nm^{-1} for low-velocity ions ($< 2 \text{ MeV u}^{-1}$ ions). As mentioned earlier, it has been reported that the track size in STO irradiated with SHIs (e.g. 2.0 GeV U ions) is similar to that in Nb-STO irradiated with the same ions. Therefore, it is reasonable to assume that the threshold S_e for track formation in Nb-STO is the same as that in STO. Based on this assumption, the threshold S_e (10 keV nm^{-1}) corresponds to the depth of 66 and 133 nm for the incidence angle of 0.5 and 1.0 degree, respectively, in the present grazing incidence condition. As demonstrated in figure 7, clear ion tracks are observable up to the depth of around 100 nm, where S_e is high enough to form ion tracks for the irradiation at 1.0 degree incidence. Therefore, the formation of observable ion tracks up to about 100 nm depth

can be explained on the basis of S_e -dependence of ion track size [17]. On the other hand, an abrupt change in track size observed in the depth range of 15–25 nm (i.e. figures 8(a)–(d) versus figure 8(e)) cannot be explained by the S_e -dependence of track size. It is attributable to the failure of recrystallization due to material deficiency as discussed above.

Finally, it is also important to point out that the material transport towards the surface observed in the present TEM results may be related to hillock chain formation. Unfortunately, *hillocks* were not observable by the present TEM observation. There is a possibility that hillocks are not contained in the very thin TEM sample used in the present study. Another possibility is that surface coating using osmium may be hindering the TEM observation of hillocks. Alternative materials such as carbon may be a better option for protective coating materials to achieve the observation of hillocks.

4. Conclusions

Hillock chains created on the surface of a single crystal of Nb-STO irradiated with 200 MeV Au^{32+} ions at grazing incidence are characterized by AFM and SEM. Exactly the same hillock chains are observed by these complementary techniques. As expected, multiple hillocks as high as around 5–6 nm are imaged by AFM. It is also found that the regions in between the adjacent hillocks are not depressed, and they are slightly elevated in many cases. AFM phase images and SEM images demonstrate the formation of line-like contrasts along the ion paths, suggesting the formation of continuous ion tracks even for the grazing incidence condition. The present results can be interpreted in the framework of the preexisting model assuming periodically peaked energy deposition, while the model assuming Rayleigh instability comes into question.

Cross-sectional TEM observation shows that the ion tracks in the near-surface region are relatively large and are deformed towards the surface, whereas ion tracks in the deeper regions are relatively small and are not deformed. The results suggest that recrystallization plays an important role in the formation of small ion tracks in the deeper regions. On the other hand, the formation of large and deformed ion tracks in the near-surface region is likely due to the failure of recrystallization which is closely related to material transport towards the surface during transient melting.

Acknowledgments

The authors are grateful to the technical staff of the accelerator facilities at JAEA-Tokai for supplying high-quality ion beams. The authors thank A Kitamura for the generous support for the research. Part of the present work was financially supported by JSPS KAKENHI Grant Number 20K05389. The authors acknowledge funding from the Austrian FWF (Project no. Y1174-N36).

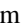
Data availability statement

All data that support the findings of this study are included within the article (and any supplementary files).

ORCID iDs

N Ishikawa  <https://orcid.org/0000-0002-2217-3645>

G L Szabo  <https://orcid.org/0000-0002-9203-4253>

R A Wilhelm  <https://orcid.org/0000-0001-9451-5440>

References

- [1] Toulemonde M, Assmann W, Dufour C, Meftah A and Trautmann C 2012 Nanometric transformation of the matter by short and intense electronic excitation: experimental data versus inelastic thermal spike model *Nucl. Instrum. Methods Phys. Res. B* **277** 28–39
- [2] Szenes G 2011 Comparison of two thermal spike models for ion–solid interaction *Nucl. Instrum. Methods Phys. Res. B* **269** 174–9
- [3] Itoh N, Duffy D M, Khakshouri S and Stoneham A M 2009 Making tracks: electronic excitation roles in forming swift heavy ion tracks *J. Phys.: Condens. Matter* **21** 474205
- [4] Aumayr F, Facsko S, El-Said A S, Trautmann C and Schleberger M 2011 Single ion induced surface nanostructures: a comparison between slow highly charged and swift heavy ions *J. Phys.: Condens. Matter* **23** 393001
- [5] El-Said A S, Aumayr F, Della-Negra S, Neumann R, Schwartz K, Toulemonde M, Trautmann C and Voss K-O 2007 Scanning force microscopy of surface damage created by fast C₆₀ cluster ions in CaF₂ and LaF₃ single crystals *Nucl. Instrum. Methods Phys. Res. B* **256** 313–8
- [6] Muller C, Voss K O, Lang M and Neumann R 2003 Correction of systematic errors in scanning force microscopy images with application to ion track micrographs *Nucl. Instrum. Methods Phys. Res. B* **212** 318–25
- [7] Popok V N, Jensen J, Vuckovic S, Macková A and Trautmann C 2009 Formation of surface nanostructures on rutile (TiO₂): comparative study of low-energy cluster ion and high-energy monoatomic ion impact *J. Phys. D: Appl. Phys.* **42** 205303
- [8] Meftah A, Benhacine H, Benyagoub A, Grob J, Izerrouken M, Kadid S, Khalfaoui N, Stoquert J, Toulemonde M and Trautmann C 2016 Data consistencies of swift heavy ion induced damage creation in yttrium iron garnet analyzed by different techniques *Nucl. Instrum. Methods Phys. Res. B* **366** 155–60
- [9] Khalfaoui N, Rotaru C, Bouffard S, Toulemonde M, Stoquert J, Haas F, Trautmann C, Jensen J and Dunlop A 2005 Characterization of swift heavy ion tracks in CaF₂ by scanning force and transmission electron microscopy *Nucl. Instrum. Methods Phys. Res. B* **240** 819–28
- [10] Khalfaoui N, Rotaru C, Bouffard S, Jacquet E, Lebius H and Toulemonde M 2003 Study of swift heavy ion tracks on crystalline quartz surfaces *Nucl. Instrum. Methods Phys. Res. B* **209** 165–9
- [11] Awazu K, Wang X, Fujimaki M, Komatsubara T, Ikeda T and Ohki Y 2006 Structure of latent tracks in rutile single crystal of titanium dioxide induced by swift heavy ions *J. Appl. Phys.* **100** 044308
- [12] Muller C, Cranney M, El-Said A, Ishikawa N, Iwase A, Lang M and Neumann R 2002 Ion tracks on LiF and CaF₂ single crystals characterized by scanning force microscopy *Nucl. Instrum. Methods Phys. Res. B* **191** 246–50
- [13] Akcöltekin E, Peters T, Meyer R, Duvenbeck A, Klusmann B, Monnet I, Lebius H and Schleberger M 2007 Creation of multiple nanodots by single ions *Nat. Nanotech.* **2** 290–4
- [14] Akcöltekin E, Akcöltekin S, Osmani O, Duvenbeck A, Lebius H and Schleberger M 2008 Swift heavy ion irradiation of SrTiO₃ under grazing incidence *New J. Phys.* **10** 053007
- [15] Akcöltekin S, Akcöltekin E, Roll T, Lebius H and Schleberger M 2009 Patterning of insulating surfaces by electronic excitation *Nucl. Instrum. Methods Phys. Res. B* **267** 1386–9
- [16] Osmani O, Duvenbeck A, Akcöltekin E, Meyer R, Lebius H and Schleberger M 2008 Calculation of electronic stopping power along glancing swift heavy ion tracks in perovskites using *ab initio* electron density data *J. Phys.: Condens. Matter* **20** 315001
- [17] Karlušić M, Akcöltekin S, Osmani O, Monnet I, Lebius H, Jakšić H and Schleberger M 2010 Energy threshold for the creation of nanodots on SrTiO₃ by swift heavy ions *New J. Phys.* **12** 043009
- [18] Karlušić M, Bernstorff S, Siketić Z, Šantić B, Bogdanović-Radović I, Jakšić M, Schleberger M and Buljan M 2016 Formation of swift heavy ion tracks on rutile TiO₂(001) surface *J. Appl. Cryst.* **49** 1704–12
- [19] Karlušić M, Jakšić M, Lebius H, Ban-d'Etat B, Wilhelm R A, Heller R and Schleberger M 2017 Swift heavy ion track formation in SrTiO₃ and TiO₂ under random channeling and near-channeling conditions *J. Phys. D: Appl. Phys.* **50** 205302
- [20] Carvalho A M J F, Marioni M, Touboul A D, Guasch C, Lebius H, Ramonda M, Bonnet J and Saigné F 2007 Discontinuous ion tracks on silicon oxide on silicon surfaces after grazing angle heavy ion irradiation *Appl. Phys. Lett.* **90** 073116
- [21] Carvalho A M J F, Touboul A D, Marioni M, Guasch C, Ramonda M, Lebius H, Saigné F and Bonnet J 2008 Single swift heavy ion-induced trail of discontinuous nanostructures on SiO₂ surface under grazing incidence *Thin Solid Films* **517** 289–92
- [22] Kitamura A, Ishikawa N, Kondo K, Yamamoto S and Yamaki T 2019 FE-SEM observation of chains of nanohillocks in SrTiO₃ and Nb-doped SrTiO₃ surfaces irradiated with swift heavy ions *Nucl. Instrum. Methods Phys. Res. B* **460** 175–9
- [23] Karczewski J, Riegel B, Gazda M, Jasinski P and Kusz B 2009 Electrical and structural properties of Nb-doped SrTiO₃ ceramics *J. Electroceramics* **24** 326–30
- [24] Li W et al 2013 Effect of doping on the radiation response of conductive Nb–SrTiO₃ *Nucl. Instrum. Methods Phys. Res. B* **302** 40–7
- [25] Ishikawa N, Taguchi T and Ogawa H 2020 Comprehensive understanding of hillocks and ion tracks in ceramics irradiated with swift heavy ions *Quantum Beam Sci.* **4** 43
- [26] Ochedowski O, Marinov K, Wilbs G, Keller G, Scheuschner N, Severin D, Bender M, Maultzsch J, Tegude F J and Schleberger M 2013 Radiation hardness of graphene and MoS₂ field effect devices against swift heavy ion irradiation *J. Appl. Phys.* **113** 214306
- [27] Ziegler J F, Biersack J P and Littmark U 1985 *The Stopping and Range of Ions in Solids* (New York, NY: Pergamon)
- [28] Ziegler J F 2004 SRIM-2003 *Nucl. Instrum. Methods B* **219–220** 1027–36
- [29] El-Said A S, Aumayr F, Della-Negra S, Neumann R, Schwartz K, Toulemonde M, Trautmann C and Voss K O 2007 Scanning force microscopy of surface damage created by fast C₆₀ cluster ions in CaF₂ and LaF₃ single crystals *Nucl. Instrum. Methods Phys. Res. B* **256** 313–8

- [30] Müller C, Voss K O, Lang M and Neumann R 2003 Correction of systematic errors in scanning force microscopy images with application to ion track micrographs *Nucl. Instrum. Methods Phys. Res. B* **212** 318–25
- [31] Popok V N, Jensen J, Vučković S, Mackova A and Trautmann C 2009 Formation of surface nanostructures on rutile (TiO₂): comparative study of low-energy cluster ion and high-energy monoatomic ion impact *J. Phys. D: Appl. Phys.* **42** 205303
- [32] Meftah A, Benhacine H, Benyagoub A, Grob J J, Izerrouken M, Kadid S, Khalfaoui N, Stoquert J P, Toulemonde M and Trautmann C 2016 Data consistencies of swift heavy ion induced damage creation in yttrium iron garnet analyzed by different techniques *Nucl. Instrum. Methods Phys. Res. B* **366** 155–60
- [33] Rayleigh W 1878 On the stability, or instability, of certain fluid motions *Proc. London. Math. Soc.* **10** 4–13
- [34] Rymzhanov R A, Medvedev N, O'Connell J H, Van Vuuren A J, Skuratov V A and Volkov A 2019 Recrystallization as the governing mechanism of ion track formation *Sci Rep.* **9** 3837
- [35] Rymzhanov R A, O'Connell J, Van Vuuren A J, Skuratov V A, Medvedev N and Volkov A 2020 Insight into picosecond kinetics of insulator surface under ionizing radiation *J. Appl. Phys.* **127** 015901
- [36] Jiang W, Devanathan R, Sundgren C, Ishimaru M, Sato K, Varga T, Manandhar S and Benyagoub A 2013 Ion tracks and microstructures in barium titanate irradiated with swift heavy ions: a combined experimental and computational study *Acta Mater.* **61** 7904–16
- [37] Zhang J, Lang M, Ewing R C, Devanathan R, Weber W J and Toulemonde M 2010 Nanoscale phase transitions under extreme conditions within an ion track *J. Mater. Res.* **25** 1344–51
- [38] Ishikawa N, Taguchi T and Okubo N 2017 Hillocks created for amorphizable and non-amorphizable ceramics irradiated with swift heavy ions: TEM study *Nanotechnology* **28** 445708
- [39] Ishikawa N, Okubo N and Taguchi T 2015 Experimental evidence of crystalline hillocks created by irradiation of CeO₂ with swift heavy ions: TEM study *Nanotechnology* **26** 355701
- [40] O'Connell J H, Skuratov V A, Akilbekov A, Zhumazhanova A and Van Vuuren, A J 2016 EM study of latent track morphology in TiO₂ single crystals. *Nucl. Instrum. Methods Phys. Res. B* **379** 200–5
- [41] Weber W J, Zarkadoula E, Pakarinen O H, Sachan R, Chisholm M F, Liu P, Xue H, Jin K and Zhang Y 2015 Synergy of elastic and inelastic energy loss on ion track formation in SrTiO₃ *Sci. Rep.* **5** 7726
- [42] Trachenko K 2004 Understanding resistance to amorphization by radiation damage *J. Phys.: Condens. Matter.* **16** R1491–515
- [43] Lang M, Djurabekova F, Medvedev N, Toulemonde M and Trautmann C 2020 Fundamental phenomena and applications of Swift heavy ion irradiations *Comprehensive Nuclear Materials* 2nd edn arXiv:2001.03711